Supporting Information for

A hierarchical WC/NiCoW hollow nanotube array as a highly efficient electrocatalyst for hydrogen evolution

Xuesong Liu,[a] Kuan Deng,[a] Peng Liu,[a] Xingbin Lv,[b] Wen Tian, [a,] Junyi Ji[a,]**

[a] School of Chemical Engineering, Sichuan University, Chengdu 610065, P. R. China.

E-mail: junyiji@scu.edu.cn

[b] College of Chemistry and Environment, Southwest Minzu University, Chengdu, Sichuan 610041, P. R. China

Corresponding author: E-mail

Wen Tian: tianwen591@scu.edu.cn

Junyi Ji: junyiji@scu.edu.cn

Supplementary Experimental Section

Preparation of CoCH/CC and Ni-$CoWO_4$/CC: All the raw materials purchased from Aladdin Co. were used directly without any further purification. In a typical process, the carbon cloth (2×3 cm, WOS 1011, CeTech Co. Ltd, China) was cleaned with ethanol and deionized water respectively, and then immersed in saturated KMnO4 for 1 h for preprocessing to provide the growth seed crystal. $Co(NO_3)_2{\cdot}6H_2O$ (2 mmol), NH_4F (4 mmol), and CH_4N_2O (10 mmol) were added into 40 mL deionized water with vigorous stirring for 10 min, the resulting solution and the treated carbon cloth were transferred to an autoclave and kept at 120 ℃ for 6 h. After the first hydrothermal reaction, the obtained CoCH/CC were used as the substrate for the second hydrothermal reaction. Briefly, $Na_2WO_4{\cdot}2H_2O$ (1.33 mmol) and $NiCl_2{\cdot}6H_2O$ (1.33 mmol) were all dissolved in 40 mL deionized water with stirring. Then 40 mL milky green solution and CoCH/CC were transferred into an autoclave and maintained at 150 ℃ for 10 h. After natural cool down, the obtained Ni-$CoWO_4$/CC precursor was taken out and washed, and then dried at 60 ℃ for 6 h under vacuum.

Preparation of WC/NCW-*x*: The Ni-$CoWO_4$/CC precursors catalyzed *in-situ* growth were conducted in a tube furnace. Firstly, the Ni-$CoWO_4$/CC composite was calcinated from room temperature to 450 ℃ with a heating rate of 3 ℃ min^{-1} in a H_2/Ar (10:90) atmosphere and kept for 1.5 h. Then, the pre-reduced composite was heated to 600 ℃ rapidly within 10 min under the same atmosphere. After that, the Ar was cut off and the H_2, CH_4, and NH_3 mixture (4:4:2) was injected under different temperatures (500, 550, 600, 650, and 700 ℃) under 200 mbar. Finally, the H_2, CH_4, and NH_3 was cut off and Ar was injected and cool naturally to room temperature to obtain the WC/NCW-*x* (*x* = 500, 550, 600, 650, and 700 ℃).

Preparation of Pt/C. To compare with the commercial Pt/C electrocatalysts, the catalyst ink of Pt/C was prepared by adding 5 mg Pt/C (20 wt.%) in a mixture of 240 μL isopropanol, 40 μL Nafion (5 wt.%), and 720 μL deionized water. Then the mixture was ultrasonicated for 30 min. The obtained catalyst ink was dropped onto the carbon cloth electrode and dried at room temperature.

Characterization. The surface morphology and microstructure of the catalysts was characterized by scanning electron microscope (SEM, JEOL JSM 7610F), energy dispersive X-ray spectroscopy (EDS) and transmission electron microscope (TEM, FEI Tecnai G20). The crystalline structures and chemical valance states were identified by X-ray diffraction (XRD, Cu Kα radiation, λ = 0.154 nm, scanned from 10° to 80°, SmartLab, Rigaku) and X-ray photoelectron spectroscopy (XPS, PHI5000 Versa spectrometer, and the binding energy was calibrated according to the reference C 1 s peak at 284.8 eV). The ex-situ Raman spectra were recorded in confocal geometry using a Cobolt CW DPSS laser emitting at 532 nm and a Renishaw InVia spectrometer equipped with a Peltier-cooled charge-coupled device detector (CCD) with a grating of 1800 L mm^{-1} and a microscope. A ×50 objective (Leica) was used for focusing. *In-situ* Raman spectra were acquired by the same Raman spectroscopy under controlled potential and performed with a custom-made spectro-electrochemical cell. The obtained electrocatalysts fixed on a copper sheet served as the working electrode and the laser shined through a quartz window onto the working electrode surface. A Pt wire and Ag/AgCl electrode were used as the counter electrode and reference electrode, respectively. The electrolyte was 0.1 M KOH. The electrochemical activities were measured in a three-electrode configuration at room temperature by CHI760E electrochemical workstation (Shanghai Chenhua Instrument Co., Ltd). In order to identify detectable interfacial species during gas evolution, Raman spectra were collected with different bias on electrode surface at the same position by chronoamperometry test.

Electrochemical measurement. The electrocatalytic performances of the HER were measured using an electrochemical station (CHI760E, Shanghai Chenhua Instrument Co., Ltd). These half-reactions were carried out in a standard three-electrode system with the electrodes as working electrode, graphite rods as counter electrode, and Hg/HgO electrodes (Ag/AgCl was used as a reference electrode in acidic and neutral electrolytes.) as reference electrode. All samples were scanned by cyclic voltammetry (CV) at 50 mV s^{-1} to obtain stable response current. All the measured potentials (vs.

reference electrode) were calculated with respect to reversible hydrogen electrode (RHE) by the Nernst equation ($E_{RHE} = E_M + 0.059 \times pH + E_R$), where E_M was the measured potentials, while E_R was 0.098 V for Hg/HgO. The linear sweep voltammetry (LSV) curves were tested at 2 mV s^{-1} with iR correction (The ohmic potential drop on the electrolyte resistance had been subtracted according to the equation: $E_{compensated} = E_M - i \times R_S$, R_S was determined by electrochemical impedance spectroscopy, EIS). Tafel plots were fitted to the equation of $\eta = a + b * \log j$, where η was the measured potential (vs. RHE), j was the current density, and b was the Tafel slope, respectively. EIS spectra were recorded with frequency from 0.01 Hz to 100 kHz at an overpotential of 300 mV for HER using an electrochemical station (Metrohm Autolab M204). The double-layer capacitance (C_{dl}) which was proportional to the effective electrochemical double layer capacitance (ECSA), was measured by a typical CV test at different scan rates from 10 mV s^{-1} to 100 mV s^{-1} in the potential range of non-Faradaic region. The electrolyte was 1.0 M KOH (pH = 14.0), 1.0 M PBS (pH = 7.0) or 0.5 M H_2SO_4 (pH = 0.3) aqueous solution.

Assessment of turnover frequency (TOF). The number of active sites should be determined by the CV curves recorded between 0 and 0.8 V (vs. RHE) in 1.0 M PBS buffer solution (pH = 7.0) at a scan rate of 50 mV s^{-1}. The number of active sites (n) is calculated at non-Faradaic region in near-neutral pH solution according to the following equation:

$$n = Q \tag{1}$$

Where Q represents whole charge calculated from CV curve (C), α represents the number of transfer electrons corresponding to the half-reaction, and F represents Faraday constant (96485 C mol^{-1}).

After calculating the number of active sites, the per-site turnover frequencies (in s^{-1}) were calculated with the following equation:

$$TOF = I/\alpha Fn \tag{2}$$

I represents the current during the LSV measurement (A) at a given overpotential,

and n is the number of active sites calculated in the previous step.

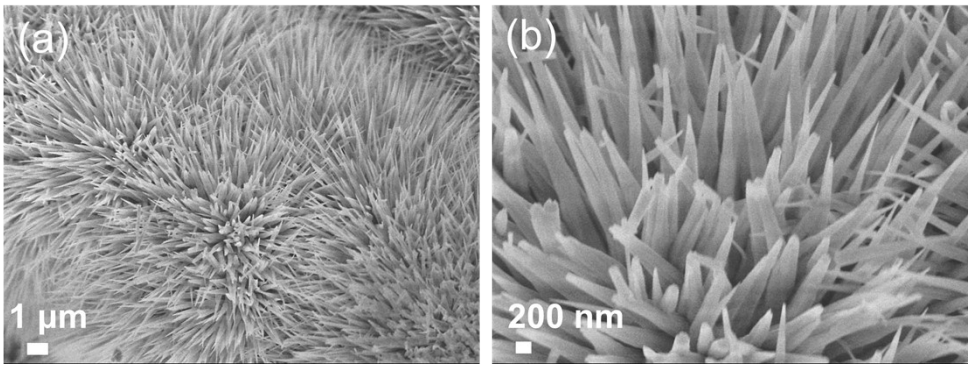

Fig. S1. SEM images of the (a, b) CoCH/CC precursors.

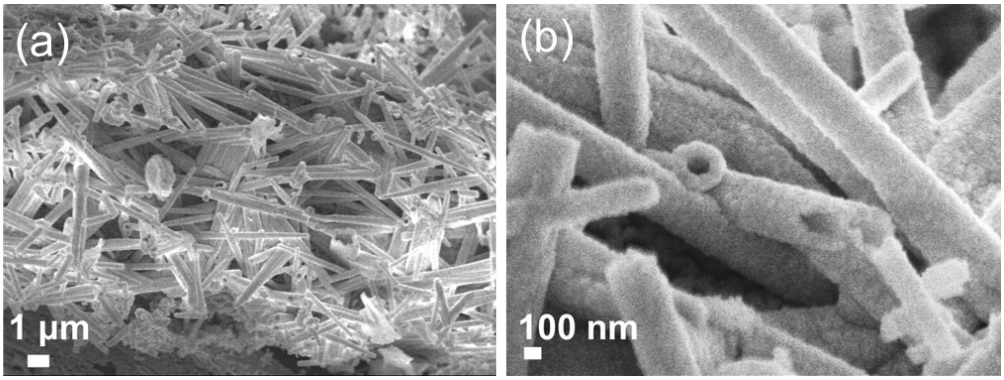

Fig. S2. SEM images of the (a, b) Ni-$CoWO_4$/CC composites.

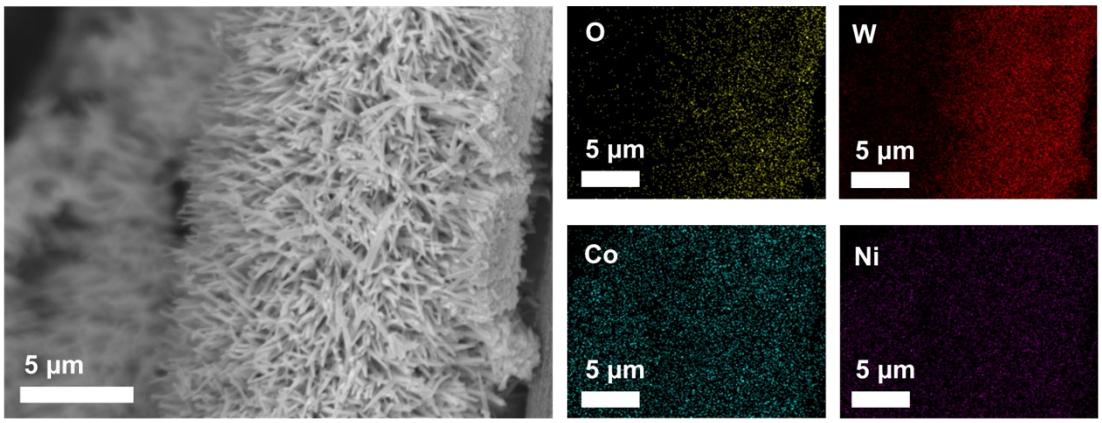

Fig. S3. EDS mappings of the Ni-$CoWO_4$/CC composites.

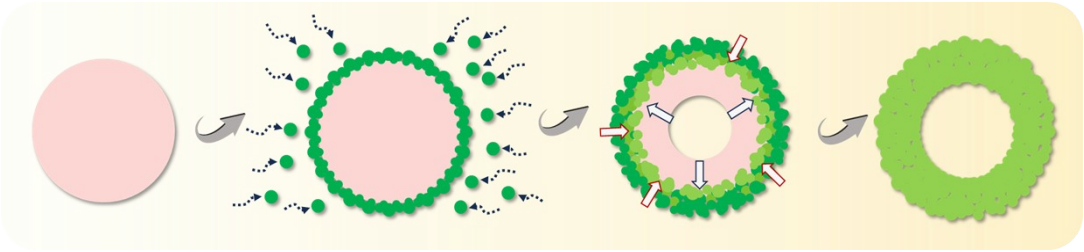

Fig. S4. Schematic of the ion exchange process

The formation of the hollow nanotube structure in WC/NCW is primarily driven by an ion-exchange process during hydrothermal treatment. Initially, the hydrothermal treatment facilitates the growth of Ni and W-based precursors on CoCH nanowires, allowing the establishment of a solid architecture. With the prolonged hydrothermal time, the interaction of Co and WO_4^{2-} species leads to the outward migration of Co-based components and the inward migration of WO_4^{2-} ions, resulting in the structural change and formation of the hollow structure, which is characteristic of the Kirkendall effect. This effect plays a significant role in shaping the hollow nanotube morphology, which provides an enhanced accessible surface area for catalytic reactions.

The subsequent high-temperature CVD process further induces phase transformations, where the Ni-$CoWO_4$-based precursor is converted into active tungsten carbide (WC) and NiCoW alloyed phases. During this process, the carbonization and carburization reactions occur, facilitated by the reducing atmosphere and the presence of carbon-containing gases, leading to the formation of the WC phase. The introduction of the tungsten carbide species results in a platinum-like electronic structure that enhances the catalytic properties by coupling with the highly electron conductive alloyed phases, thus creating highly active sites for electrocatalysis.

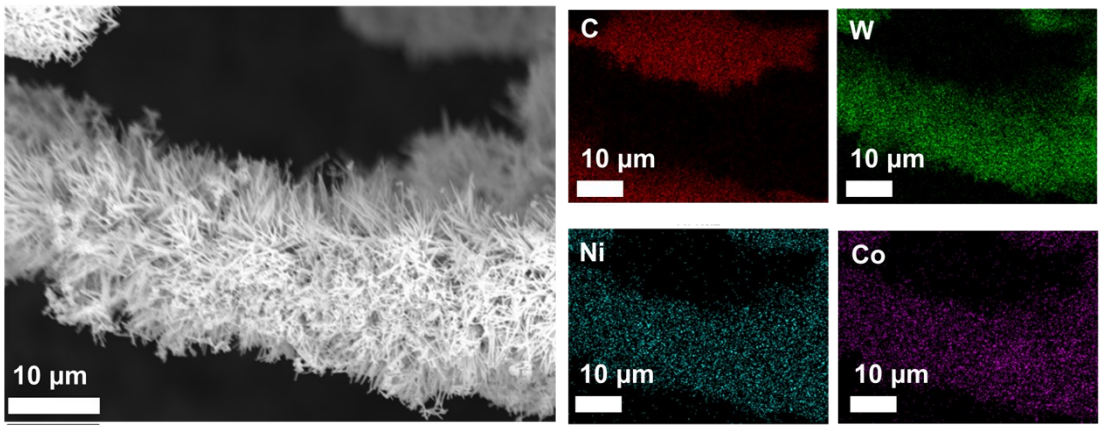

Fig. S5. EDS mappings of the WC/NCW-600 composites.

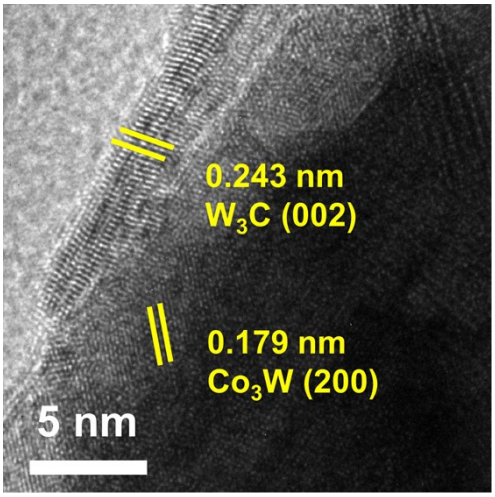

Fig. S6. TEM images of WC/NCW-600.

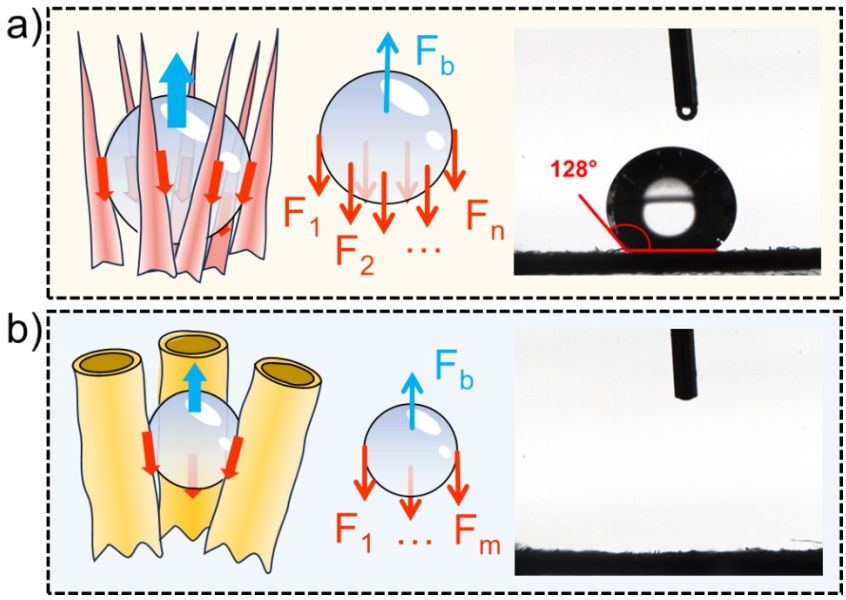

Fig. S7. Graphical illustration of gas bubble adhesion behavior on (a) CoCH nanoneedle array and (b) WC/NCW nanotube array, along with corresponding contact angle images.

The tubular structure of WC/NCW significantly enhances catalytic performance through two primary mechanisms: improved wettability and reduced bubble adhesion force.

First, the water wettability of the hollow nanotube structure is enhanced due to the increased surface roughness, which can be described by the Wenzel model.[1]

$\cos(\theta^*) = r * \cos(\theta)$

According to the Wenzel equation, the apparent contact angle (θ^*) on a rough surface is reduced with the increase of roughness factor ($r > 1$). This increased roughness results in complete superhydrophilicity, as indicated by the measured contact angle of 0° for the WC/NCW sample, which facilitates rapid gas bubble detachment during catalytic reactions due the superphobicity.

Second, as shown in **Fig. S7**, the CoCH nanoneedle array with large interspace can maintain larger bubble size and create higher adhesion force (F_n) between the bubbles and solid surface due the ultrasmall diameter and smooth surface, which is much larger compared to the hollow nanotube array with increased diameter (F_m). Therefore, the rough surface and decreased gas-solid contact area in the hollow nanotube array can

synergistically enhance the superaerophobicity, which result in smaller bubble size, faster bubble detachment, and reduced resistance during catalytic operation, as evidenced by our bubble release videos. This improved bubble release dynamics contributes to faster mass transfer and increased catalytic efficiency/stability, thereby enhancing the overall catalytic performance.

These combined effects, the enhanced wettability and reduced bubble adhesion, significantly improve gas escape efficiency, leading to superior catalytic activity and stability under reaction conditions.

[1] X. Dai, B. B. Stogin, S. Yang and T.-S. Wong, ACS Nano, 2015, 9, 9260-9267.

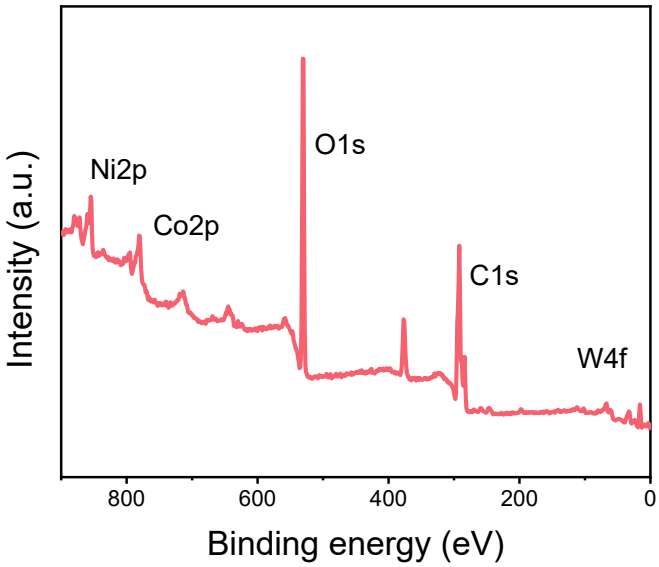

Fig. S8. XPS full surveys of the as-prepared WC/NCW-600.

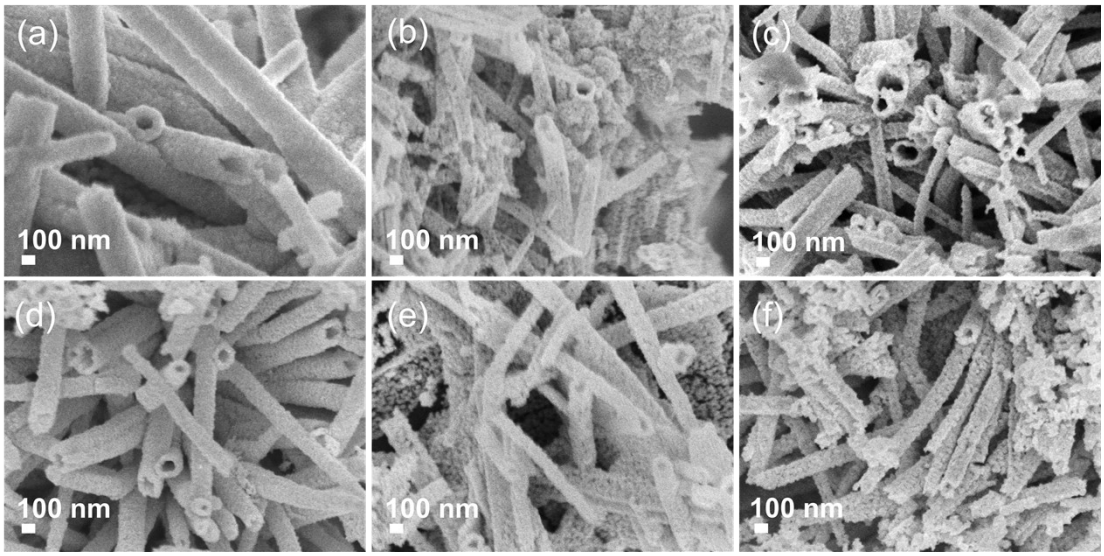

Fig. S9. SEM images of the (a) Ni-$CoWO_4$/CC, (b) WC/NCW-500, (c) WC/NCW-550, (d) WC/NCW-600, (e) WC/NCW-650, and (f) WC/NCW-700.

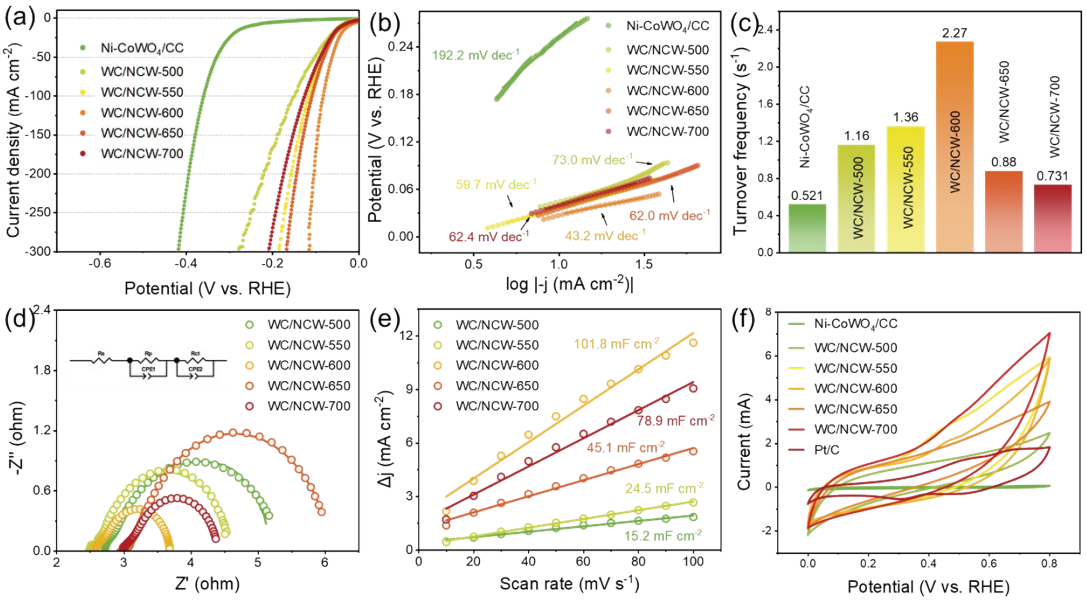

Fig. S10. (a) LSV curves, (b) Tafel plots, (c) TOF values, (d) Nyquist plots, and (e) C_{dl} values of Ni-$CoWO_4$/CC and WC/NCW-*x* electrodes in 1.0 M KOH. (f) CV curves in 1.0 M PBS are calculated for TOF values of Ni-$CoWO_4$/CC, WC/NCW-*x*, and Pt/C electrodes.

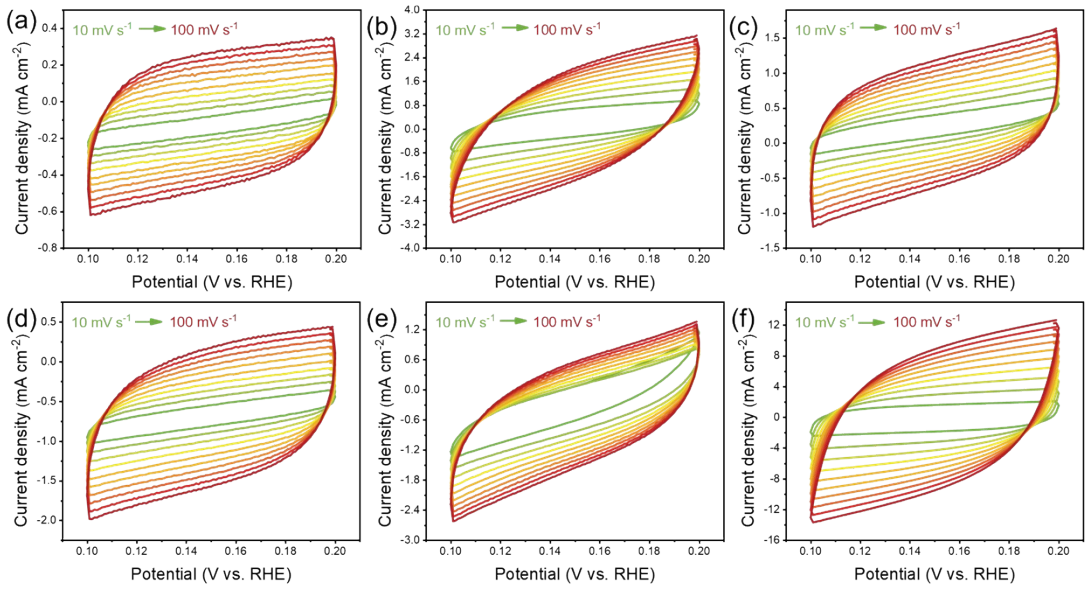

Fig. S11. Cyclic voltammetry curves of the (a) Ni-$CoWO_4$/CC, (b) WC/NCW-500, (c) WC/NCW-550, (d) WC/NCW-600, (e) WC/NCW-650, and (f) WC/NCW-700 in 1.0 M KOH at different scan rates from 10 mV s^{-1} to 100 mV s^{-1}.

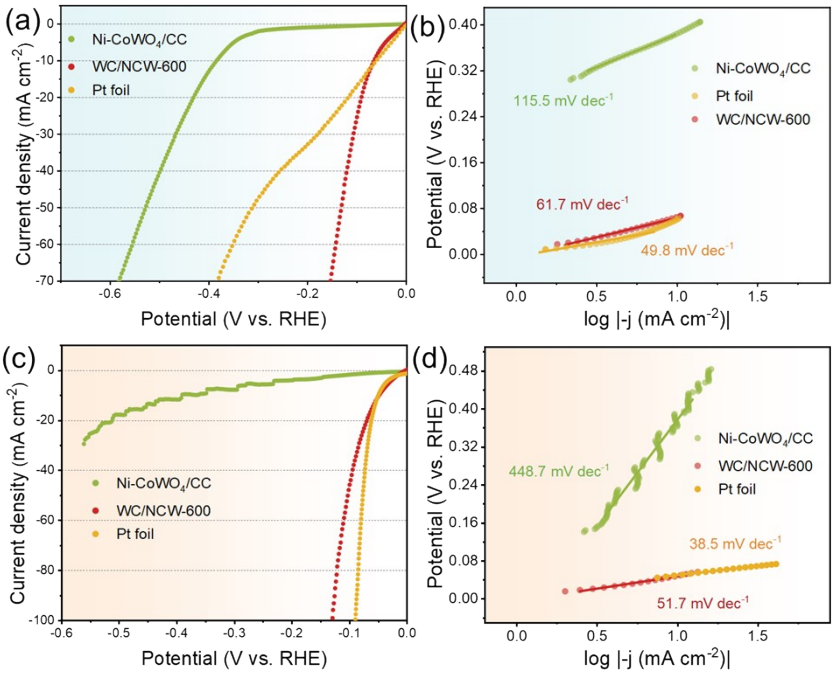

Fig. S12. (a) LSV curves and (b) Tafel plots of Ni-$CoWO_4$/CC, Pt foil, and WC/NCW-600 electrode in 1.0 M PBS. (c) LSV curves and (d) Tafel plots of Ni-$CoWO_4$/CC, Pt foil, and WC/NCW-600 electrode in 0.5 M H_2SO_4.

Table S1. The values of fitted equivalent circuit parameters of the Ni-$CoWO_4$/CC, WC/NCW-500, WC/NCW-550, WC/NCW-600, WC/NCW-650, and WC/NCW-700 electrodes in HER.

Electrode materials	**R_s (Ω)**	**R_p (Ω)**	**R_{ct} (Ω)**
Ni-$CoWO_4$/CC	3.296	0.237	9.784
WC/NCW-500	2.705	0.096	2.555
WC/NCW-550	2.505	0.176	1.934
WC/NCW-600	2.569	0.217	0.902
WC/NCW-650	3.000	0.223	2.871
WC/NCW-700	2.976	0.255	1.174